Surfactant-Templated Synthesis and Catalytic Properties of Patterned Nanoporous Titania Supports Loaded with Platinum Nanoparticles

Jayashri Sarkar,[†] Vijay T. John,[‡] Jibao He,[‡] Christopher Brooks,[§] Darshan Gandhi,[||] Anthony Nunes,[⊥] Ganapathiraman Ramanath,[||] and Arijit Bose*,[†]

Department of Chemical Engineering, University of Rhode Island, Kingston, Rhode Island 02881, Department of Chemical Engineering, Tulane University, New Orleans, Louisiana 70118, Honda Research Institute, Columbus, Ohio 43212, Materials Science and Engineering Department, Rensselaer Polytechnic Institute, Troy, New York 12180, and Department of Physics, University of Rhode Island, Kingston, Rhode Island 02881

Received May 22, 2008

Hexagonally patterned porous titania is synthesized from a titanium isopropoxide precursor using a viscous surfactant template separating nanoscopic bicontinuous channels of water and isooctane. Subsequent salt reduction in the aqueous nanochannels decorates the pore surfaces with well-separated platinum (Pt) nanoparticles. Because of the decreased mass transfer resistance provided by the patterned and interconnected macropores that persist throughout the support, these nanocomposites exhibit a significantly higher carbon monoxide oxidation efficiency than that obtained with a commercial support that has a fourfold larger specific surface area. This simple templated synthesis strategy for creating highly organized composites has wide applications beyond the one reported here, including photocatalysis, photonic crystals, sensors, and solar cell assemblies.

Introduction

Nanoporous titania (TiO_2) has several important optical and electronic properties that make it useful for various applications such as pigments in paints, catalyst support,[1] sensors, porcelain enamels, cosmetics, sunscreens, photocatalyst,[2–5] photovoltaic devices,[2,4–7] semiconductors,[8] and ultrahydrophobic or self-cleaning glass.[9] Anatase-based nanocomposites have been used to photocatalytically purify air and water[10,11] and obtain photonic crystals with tunable band gaps[2,12,13] and enhanced light emission.[2,14] Noble metal nanoparticles loaded on nanoporous TiO_2 supports are attractive for catalyzing reactions germane to energy generation and environmental preservation, for example, photocatalytic generation of hydrogen from water[1,2] and carbon monoxide (CO) oxidation.[15] The efficiency of TiO_2 supported catalysts is increased through electronic-structure-level interactions at the support−catalyst interface.[16–19] For example, the amount of CO converted to CO_2 per unit mass of Pt catalyst per unit time (referred to as the turnover frequency, TOF) is hundredfold higher with a TiO_2 support than with a SiO_2 support over a temperature range of 150 to 550 °C.[20–24]

* Corresponding author: Arijit Bose; email bosea@egr.uri.edu, tel: 401-874-2804, fax: 401-874-4689

[†] Department of Chemical Engineering, University of Rhode Island.

[‡] Tulane University.

[§] Honda Research Institute.

[||] Rensselaer Polytechnic Institute.

[⊥] Department of Physics, University of Rhode Island.

(1) Borgarello, E.; Kiwi, J.; Pelizzetti, E.; Visca, M.; Gratzel, M. *Nature* **1981**, *289*, 158–160.

(2) Grätzel, M. *Nature* **2001**, *414*, 338–344.

(3) Kim, T. K.; Lee, M. N.; Lee, S. H.; Park, Y. C.; Jung, C. K.; Boo, J. H. *Thin Solid Films* **2005**, *475*, 171–177.

(4) Sclooff, L. H.; Wienk, M. M.; Kroon, J. M. *Thin Solid Films* **2004**, *451−452*, 634–638.

(5) Wang, H.; Oey, C. C.; Djurisic, A. B.; Xie, M. H.; Leung, Y. H.; Man, K. K. Y.; Chan, W. K.; Pandey, A.; Nunzi, J. M.; Chui, P. C. *Appl. Phys. Lett.* **2005**, *87*, 023507. (023501−023503).

(6) Kim, Y.-G.; Samuelson, L. A.; Walker, J.; Kumar, J. Efficient light harvesting polythiophenes for nanocrystalline TiO2 photovoltaic cells *Abstracts of Papers*, 224th ACS National Meeting, Boston, MA, August 18−22, 2002; American Chemical Society: Washington, DC, 2002; POLY-605.

(7) Kim, Y.-G.; Mosurkal, R.; Samuelson, L. A.; Walker, J.; Li, L.; Kumar, J. Synthesis and characterization of functional ruthenium dyes for nanocrystalline TiO2 photovoltaic cells *Abstracts of Papers*, 224th ACS National Meeting, Boston, MA, August 18−22, 2002; American Chemical Society: Washington, DC, 2002; INOR-417.

(8) Yamada, H.; Yamato, t.; Moriguchi, I.; Kudo, T. *Solid State Ionics* **2004**, *175*, 195–198.

(9) Blossey, R. *Nature* **2003**, *2*, 301–306.

(10) Mills, A.; LeHunte, S. *J. Photochem. Photobiol., A* **1997**, *108*, 1.

(11) Fujishima, A.; Rao, T. N.; Tyrk, D. A. *J. Photochem. Photobiol., C* **2000**, *1*, 1.

(12) Subramanian, G.; Manoharan, V. N.; Thorne, J. D.; Pine, D. J. *Adv. Mater.* **1999**, *11*, 1261–1265.

(13) Joannopoulos, J. D.; Meade, R. D.; Winn, J. N. *Photonic Crystals*; Princeton University Press: Princeton, 1995.

(14) Hideomi, K.; Takeuchi, I. *Nature* **2004**, *3*, 429–438.

(15) Sato, T.; Koizumi, M.; Miyao, T.; Naito, S. *Catal. Today* **2006**, *111*, 164–170.

(16) Kotsifa, A.; Kondarides, D. I.; Verykois, X. E. *Appl. Catal., B* **2007**, *72*, 136–148.

(17) Wang, X.; Yu, J. C.; Yip, Y. H.; Wu, L.; Wong, P. K.; Lai, S. Y. *Chem. Eur. J.* **2005**, *11*, 2997–3004.

(18) Lee, J.; Choi, W. *J. Phys. Chem. B* **2005**, *109*, 7399–7406.

(19) Alexeev, O. S.; Chin, S. Y.; Engelherd, M. H.; Soto, L. O. *J. Phys. Chem. B* **2005**, *109*, 23430–23443.

(20) Panagiotopoulou, P.; Kondarides, D. I. *Catal. Today* **2006**, *112*, 49–52.

(21) Tauster, S. J.; Fung, S. C.; Garten, R. L. *J. Am. Chem. Soc.* **1978**, *100*, 170–175.

(22) Tauster, S. J. In *ACS Symposium Series*; Baker, R. T. K., Tauster, S. J., Dumesic, J. A., Eds.; American Chemical Society: Washington, DC, 1986; Vol. 298, p 1−221.

10.1021/cm8014034 CCC: $40.75
Published on Web 07/30/2008

Clearly, the catalyst and support chemistries, the support structure, and the catalyst particle distribution within the pores are important parameters that must be controlled to achieve a high TOF.

Several techniques have been devised to synthesize catalyst−support composites, such as impregnation,[25–27] sol−gel based processes,[28] flame spray synthesis,[29] electrodeposition,[30] laser pyrolysis,[31] sonochemistry,[32] and UV irradiation.[33] In all of these processes, the support material (usually disordered) is prepared first, followed by the transfer to, or formation of, catalyst particles within the pores. Such sequential approaches entail disadvantages such as pore plugging, insufficient control of catalyst distribution within the pores, and high costs due to production complexity. Disordered and disconnected pores in the support lead to increased mass transfer resistance. Hence, there is a need to devise simpler synthesis strategies that allow the formation of patterned and interconnected porous supports with nanoparticles of controllable size distributed throughout the support structure.

Here, we demonstrate a soft-templating technique for the synthesis of highly organized nanoporous anatase loaded with a uniform dispersion of Pt nanoparticles. To the best of our knowledge, this is the first report of a loaded catalyst composite where both the support and the catalyst are synthesized using the same soft template, at room temperature. The key feature of our approach is the ability to distribute the nanoparticles uniformly throughout the support with minimal agglomeration and pore blocking. We have characterized the catalytic activity our samples using the oxidation of CO to CO_2 and shown that the conversion efficiency of our nanocomposites for this reaction is significantly better than a commercial catalyst material with a 4-fold higher surface area. The higher efficacy of our nanocomposite is attributed to the structure of pore patterning which extends throughout the powder particles and their interconnectivity, which provides improved mass transfer[34,35] of reactants to and products from the catalyst surfaces in the pores.

Materials and Methods

Isooctane, dioctyl sulfosuccinate sodium salt (AOT), titanium isopropoxide (TIP), platinum chloride ($PtCl_4$),and sodium borohydride ($NaBH_4$) are obtained from Sigma Aldrich. Lecithin (L-α phosphatidylcholine, 95% plant Soy) is used as received from Avanti Polar Lipids.

Our synthesis scheme exploits the organization provided by a special surfactant template system. Addition of water to the isooctane/AOT/Lecithin microemulsion produces a highly viscous bicontinuous "gel" phase with nearly equal proportions of isooctane and water distributed as nanochannels.[36] The high viscosity of our template phase is important for immobilizing the support structure and the precipitated catalyst nanoparticles. In our experiments, TIP is dissolved in the organic solvent mixture prior to addition of the aqueous phase. Anatase titania is formed by the hydrolysis and condensation of TIP. Since TIP is organic-soluble and has limited solubility in water, the TiO_2 forms at the oil/water interfaces. The role of the surfactants is to organize the template but not participate in the reaction. Thus, the template remains intact and enables the TiO_2 to inherit the underlying template microstructure. For the synthesis of Pt-loaded TiO_2 composites, $PtCl_4$, a water-soluble salt precursor, is reduced using sodium borohydride to form Pt nanoparticles. The even distribution of the Pt^{4+} ions throughout the gel and its high viscosity enhance the ability of this method to produce well-distributed nanoparticles.

Porous Titania Synthesis. TIP is added in a 1:1 volume ratio with isooctane to the solution of isooctane/AOT (0.8 M)/Lecithin (0.4 M). A calculated amount of water, corresponding to the desired W_0 (the ratio of moles of water to AOT), is added to this solution and mixed using a vortex mixer. Immediately after water addition, a white precipitate is observed indicating TiO_2 formation. The samples are dried at 60 °C for 24 h and calcined by ramping the temperature in increments of 50 °C every 30 min, starting at 400 °C and going to 550 °C. The sample is left at 550 °C for 4.5 h to obtain a white powder. The calcination step eliminates the trace amounts of surfactants left after solvent removal.

Pt-Loaded Titania Nanocomposite Synthesis. An aqueous solution (0.015 M) of $PtCl_4$ is added to the TIP/isooctane/AOT/Lecithin to reach a desired W_0. Then a 0.1 M $NaBH_4$ solution is used to reduce the $PtCl_4$. Excess reducing agent is used to ensure complete reduction of the Pt^{4+} ions. The sample undergoes a color change from a light yellow to black, indicating the reduction of Pt^{4+} ions to Pt metal. The drying and calcination steps remain the same as those used for the support synthesis. One of the products of the synthesis strategy is small quantities of sodium chloride (NaCl) coming from the sodium ions associated with the reducing agent and the chloride ions associated with the platinum salt. The presence of NaCl within the pores blocks some active sites on the catalyst. Thus we have prepared some samples where we have removed this NaCl by washing with distilled deionized water five times after calcination.

Microanalytical Characterization. A Hitachi S-4800 Field Emission scanning electron microscope is used to characterize the support microstructure and nanoparticle dispersions. An Oxford INCA system is used for the EDS elemental analysis. Thin sections of samples for TEM measurements are prepared using a MT2-B DuPont Ultramicrotome by embedding the powder particles into an epoxy resin, curing overnight, and cutting 70−90 nm thick slices using a diamond knife. TEM images are obtained in a JEOL 1200 EX instrument operated at 120 kV. A Bruker D8 Advanced X-ray diffractometer is used for phase identification. Core-level spectra from the samples are obtained by XPS using a PHI 5400 instrument with a Mg Kα source. The spectra are collected using a pass energy of 23.5 eV and corrected for charging by using the adventitious carbon 1s peak at 285 eV. Hydrogen chemisorption on a Micrometrics AutoChem 2910 is used to obtain the active metal surface

(23) Han, Y.; Lui, C. J.; Ge, Q. *J. Phys. Chem. B* **2006**, *110*, 7463–7472.
(24) Ocal, C.; Ferrer, S. *J. Chem. Phys.* **1986**, *84*, 6474–6478.
(25) Liu, Z.; Guo, B.; Hong, L.; Jiang, H. *J. Photochem. Photobiol., A* **2005**, *172*, 81–88.
(26) Iida, H.; Igarashi, A. *Appl. Catal. A: General* **2006**, *298*, 152–160.
(27) Li, Y.; Xie, Y.; Peng, S. *Chemosphere* **2006**, *63*, 1312–1318.
(28) Sreethawong, T.; Yoshikawa, S. *Int. J. Hydrogen Energy* **2006**, *31*, 786–796.
(29) Teoh, W. Y.; Madler, L.; Beydoun, D.; Pratsinis, S. E.; Amal, R. *Chem. Eng. Sci.* **2005**, *60*, 5852–5861.
(30) Francioso, L.; Presicce, D. S.; Siciliano, P.; Ficarella, A. *Sens. Actuators, B: Chem.* **2007**, *123* (1), 516–521.
(31) Sophie, G.; Guillaume, L.; Hicham, M.; Nathalie, H.-B.; Sabine, V.; Erwan, G.; Jöel, B.; Zelimir, G. *J. Eur. Ceram. Soc.* **2007**, *27*, 931–936.
(32) Mizukoshi, Y.; Makise, Y.; Shuto, T.; Hu, J.; Tominaga, A.; Shironita, S.; Tanabe, S. *Ultrason. Sonochem.* **2007**, *14*, 387–392.
(33) Park, H.; Lee, J.; Choi, W. *Catal. Today* **2006**, *111*, 259–265.
(34) Goettmanna, F.; Sanchez, C. *J. Mater. Chem.* **2007**, *14*, 24–30.
(35) Wang, X.; Yu, J. C.; Ho, C.; Hou, Y.; Fu, X. *Langmuir* **2005**, *21*, 2552–2559.
(36) Simmons, B. A.; Irvin, G. C.; Agarwal, V.; Bose, A.; John, V. T.; McPherson, G. L.; Balsara, N. P. *Langmuir* **2002**, *18*, 624–632.

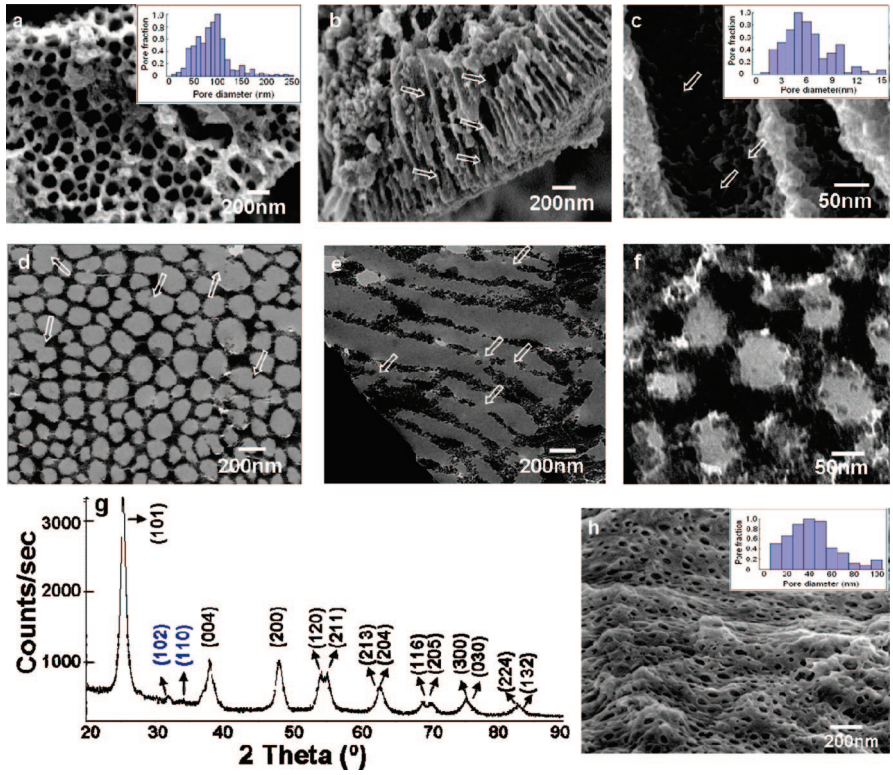

Figure 1. SEM images showing (a) cross-section and (b) longitudinal views of the pore topography for titania support obtained with $W_0 = 70$. Inset in (a) shows the macropore diameter distribution. (c) A high magnification image revealing the mesopore structure within the macropore walls; inset shows the mesopore diameter distribution. Thin section TEM images of TiO_2 supports synthesized with $W_0 = 70$ showing (d) a transverse section capturing the honeycomb microstructure, (e) a longitudinal section showing the interconnections between macropores (see arrows), and (f) macropores formed by the assembly of TiO_2 nanoparticles. (g) X-ray diffractogram of the TiO_2. The peaks correspond to the anatase phase; the small peaks marked in blue are due to Na_2SO_4, coming from the surfactant (h) a cryo-SEM image from a titania sample obtained using $W_0 = 70$, prior to solvent and surfactant removal. Inset shows the pore diameter distribution determined from the SEM images.

area and dispersion of Pt. Hydrogen reduction is first used to prepare the samples. Approximately 0.5 g of sample is loaded for each experiment and reduced in situ in a 10% H_2/90% He mix at 300 °C for 1 h. The flow is then stopped and the sample allowed to degas for 3 h at 300 °C and then brought to room temperature. The sample is then introduced to Ar carrier at 50 mL/min, and the temperature is ramped to 50 at 5 °C/min to purge any reduction products. For the pulse chemisorption experiment, H_2 is introduced using a 10% H_2/90% argon (Ar) mixture with 100% Ar as the background carrier gas. An amount of 100 μL of the mixture is dosed every 3 min until no further hydrogen was chemisorbed, and the amount of adsorbed H_2 is calculated. The Pt specific surface area (surface area of Pt/gm of Pt) and dispersion are calculated assuming a H_2/Pt stoichiometry of 2.

Catalyst Activity. We have characterized the catalytic activity of our samples for the CO to CO_2 oxidation reaction using the steady state conversion in a fixed bed reactor (eight-channel fixed-bed reactor, Celero). For the unwashed samples, 0.15 g of the nanocomposite are placed in a 3 mm reaction well. The gas mixture comprised of 1100 ppm CO, 5% O_2, and the remaining N_2 is delivered via mass flow controllers at a GHSV of 50 000 h^{-1}. For the washed samples, the conversion increased quite dramatically. To capture the details of the conversion efficiency versus temperature for those samples, we had to reduce the amount of nanocomposite to 0.05 g and use a space velocity of 300 000 h^{-1}. The gases are passed through a preheater before contacting the catalyst bed. Upon reaching the required temperature, the reaction is allowed to achieve steady state and is held at that temperature for 1 h prior to sampling. The product gases are analyzed using a gas chromatograph equipped with a methanizer and field ionization detector (Shimadzu GC-17A). The conversion is calculated based upon the CO/CO_2 ratios in the inlet and product streams.

Results and Discussion

TiO_2 supports synthesized from the soft-template using isooctane, AOT, Lecithin, TIP, and water yield a white powder. This powder consists of particles with pore diameters between 20 and 250 nm (macropores), organized with hexagonal symmetry similar to the template.[36] Figure 1a shows a SEM micrograph of a powder particle from the sample prepared using a template that had $W_0 = 70$. The average macropore diameter, obtained from the distribution, shown in the inset in Figure 1a, is ~100 nm. Due to the inheritance of the underlying bicontinuous surfactant template morphology, the macropores are interconnected through the regions marked by the arrows in Figure 1b. A higher magnification image, shown in Figure 1c, reveals the mesopores (see arrows). The average size of the mesopores determined from the SEM images is ~5 nm. BET pore diameter distribution for the same support obtained from a 55 point analysis shows the pore diameter has essentially a bimodal distribution with maxima at 3 nm and 5.5 nm, consistent with the mesopore diameter measured using SEM. Such hierarchical interconnected porous structures with a biomodal pore diameter distribution are conducive for improved access to the surfaces inside the support for both the reactants and products.

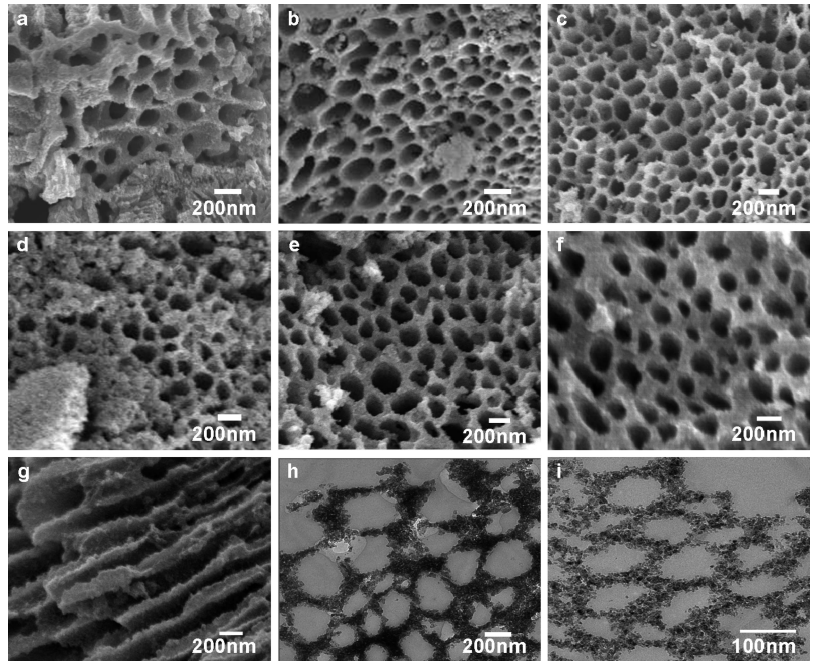

Figure 2. SEM images of TiO_2 supports prepared with (a) $W_0 = 70$, (b) $W_0 = 100$, (c) $W_0 = 130$, (d) $W_0 = 150$, (e) $W_0 = 170$, and (f) $W_0 = 200$, showing increase in the macropore diameters with increasing water content, and (g) longitudinal SEM image of a $W_0 = 200$ sample. Thin section TEM images of a $W_0 = 200$ sample (h) hexagonally organized pores. (i) A high magnification image showing individual particles.

Thin-section transmission electron microscope (TEM) images of the sample from lateral and axial cross-sections, shown in Figure 1d,e, confirm that the TiO_2 inherits the hexagonal template morphology.[36–39] Solvent removal and calcination breaks the long-range crystalline symmetry that exists in the original surfactant template, but the essentially hexagonal patterning is maintained. Images taken from a range of thin-sections taken from different portions of our samples always show this structure, and are therefore assumed to persist throughout. The breaks in the pore walls shown by the arrows in Figure 1e confirm macropore interconnectivity inside the support. Higher magnification TEM images reported in Figure 1f show that the macropore walls are comprised of an assembly of fused TiO_2 nanoparticles. Similar hierarchal microstructures, but with 10-fold larger pore diameters, have been obtained previously,[35] albeit by a completely different route.

Energy dispersive X-ray spectroscopy (see Supporting Information) shows prominent Ti and O peaks corresponding to a $TiO_{1.76}$ stoichiometry. Only trace amounts (<1.8 atomic %) of P, S, and Na from the surfactants are observed, suggesting that contamination of the pores from residual surfactants is negligible. The powder X-ray diffractogram, shown in Figure 1g, reveals that the TiO_2 in our samples is anatase, in agreement with earlier work showing that anatase is preferred at temperatures below 550 °C.[35] The peaks are broad, indicating that the crystallite size is in the support is small. The very small peaks,, marked in blue, at $2\theta \sim 30°$ are due to the presence of trace quantities Na_2SO_4, remnant from the AOT after the calcination procedure. These elements were also identified in the EDS spectra.

The characteristic macropore diameters in our TiO_2 supports are about 10-fold larger than that of the template water channels determined using small angle neutron scattering (SANS)[36] in the bicontinuous surfactant templates that contained no TIP. Cryogenic scanning electron microscope (cryo-SEM) images of TiO_2 samples prior to solvent removal shown in Figure 1h reveals macropore diameters between 20 and 150 nm, which are intermediate between the template feature sizes obtained by SANS and pore diameters of the calcined TiO_2 support measured by SEM and TEM. This observation implies that one major contributing factor to the pore diameter increase is solvent evaporation, which consolidates the TiO_2 nanoparticles into the walls by capillary forces. The solubility of AOT in TIP is 0.4 g/mL. The preferential dissolution of AOT into the TIP/isooctane solution leaves excess Lecithin at the aqueous/organic interfaces. Since Lecithin alone forms water pools of larger diameter in water-in-oil microemulsions,[40] an additional factor for the observed pore diameter is this selective loss of AOT from the isooctane/water interface. Examination of microstructures prior to and after calcination reveals only a 3% increase in macropore diameter, which is small compared to the solvent evaporation and surfactant dissolution effects.

The mean pore diameter in these support structures can be tuned without altering the qualitative features of the TiO_2 microstructure by adjusting the water content. For example, increasing the water content from $W_0 = 70$ to 200, shown

(37) Liu, L.; Li, S.; Simmons, B.; Singh, M.; John, V. T.; McPherson, G. L.; Agarwal, V.; Johnson, P.; Bose, A.; Balsara, N. *J. Dispers. Sci. Technol.* **2002**, *23*, 441–452.
(38) John, V. T.; Simmons, B.; McPherson, G. L.; Bose, A. *Curr. Opin. Colloid Interface Sci.* **2002**, *7*, 288–295.
(39) Liu, L. L., S.; Simmons, B.; Singh, M.; John, V. T.; McPherson, G. L.; Agarwal, V.; Johnson, P.; Bose, A.; Balsara, N. *J. Dispers. Sci. Technol.* **2002**, *23*, 441–452.
(40) Israelachvili, J. N. *Intermolecular and Surface Forces*, 2nd ed.; Academic Press: New York, 2002.

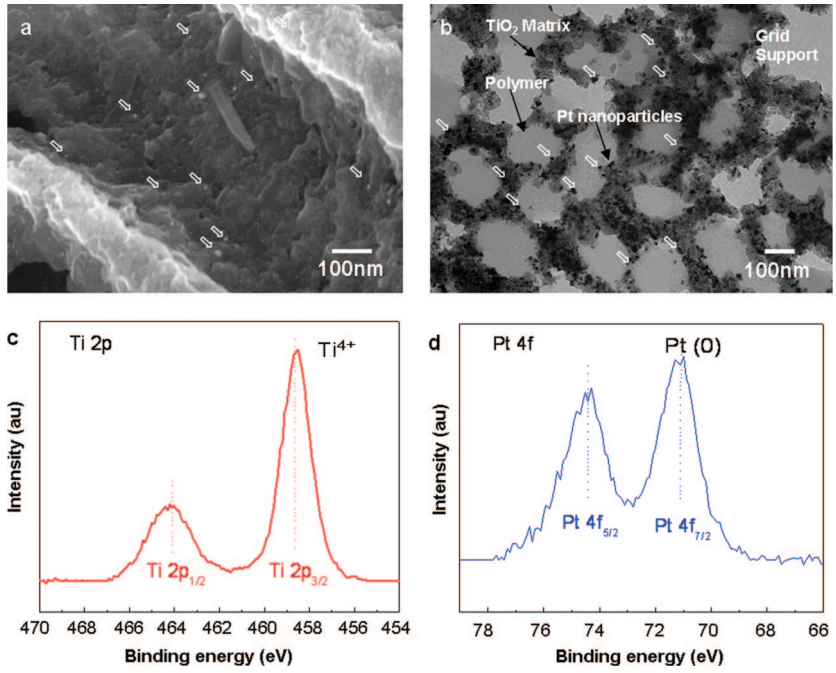

Figure 3. (a) SEM micrograph showing the surface topography and Pt nanoparticle distribution inside the titania pores for the $W_0 = 200$ nanocomposite. (b) Thin section TEM image of a $W_0 = 200$ sample showing the distribution of the ~3−5nm Pt nanoparticles (dark spots) around the surface of the macropores with no noticeable agglomeration. Core-level spectra measured by XPS showing (c) the presence of Ti^{4+} and (d) metallic platinum Pt^0.

in Figure 2, results in an increase in pore diameter from 100 to 185 nm. The internal macropore structure remains unaffected with increasing W_0. The macropore wall thickness increases with increasing W_0, primarily because additional water drives the TIP hydrolysis to completion. The BET surface area of the supports also increases marginally as the water content is enhanced, giving 24.4, 34.2, 37.6, and 41.9 m^2/g for $W_0 = 70$,100, 150, and 200, respectively.

When the titania support synthesis is carried out in the presence of a platinum salt ($PtCl_4$) solution, reduced in a subsequent step by adding sodium borohydride, we obtain TiO_2 supports decorated with 3−5 nm diameter Pt nanoparticles that are well-separated and uniformly distributed on the pore surfaces, as seen in Figure 3. The high viscosity (zero shear viscosity of ~10^5 poise) of the underlying template immobilizes the Pt nanoparticles inside the aqueous nanochannels. We note that the hexagonal patterning of the pores is preserved, indicating that the Pt salt reduction does not disrupt pore organization in the support. EDS spectra from the nanocomposite samples show prominent Ti, O, and Pt peaks, along with trace amounts (<1.8%) of P and S from the surfactants (data not shown). The specific surface areas for the nanocomposites are 22.3, 26.9, and 36.9 m^2/g for samples of $W_0 = 70$, 100, and 200 respectively. The surface area of the support is essentially unaffected by the addition of Pt in the support. X-ray photoelectron spectroscopy (XPS) scans in the vicinity of the Ti 2p and Pt 4f core-level bands are shown in Figure 2c,d. The Ti $2p_{3/2}$ band at 458.5 eV corresponds to the Ti^{4+} state,[41] while the Pt $4f_{7/2}$ band at 71.1 eV is in good agreement with the Pt^0 state.[18] The reaction products are thus titania and metallic platinum.

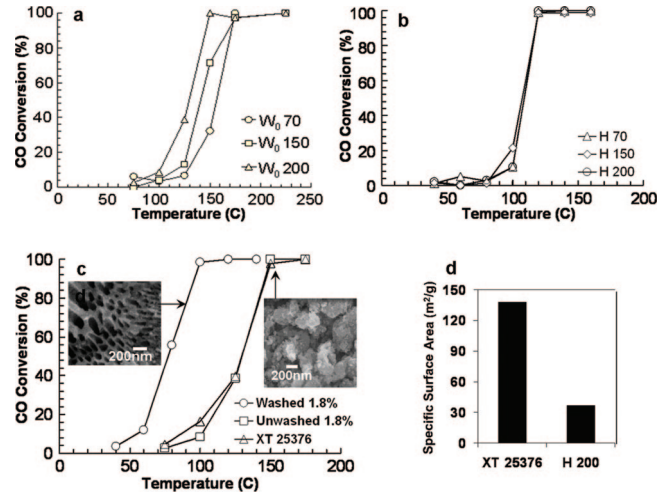

Figure 4. (a) Carbon monoxide to carbon dioxide conversion efficiency characteristics for TiO_2/Pt nanocomposites with Pt contents (wt %) of 0.5% (○), 1.5% (□), and 1.8% (Δ), respectively. (b) Activity at similar Pt loading on supports with varying W_0 from 70 to 200 showing negligible effect on catalysis. (c) Comparison of the conversion characteristics of our organized unwashed nanocomposite (□) and washed nanocomposite (○) with that of the commercial (XT 25376 from St. Gobain-Norpro) sample (Δ) with equivalent Pt loadings of 1.8 wt %. SEM images from the commercial sample XT 25376 from St. Gobain-Norpro show a highly disorganized pore structure, in contrast to the highly organized pores in our sample. (c) Comparison of the specific surface areas of our organized titania samples with that of the St. Gobain sample shows a fourfold lower surface area in the samples prepared by our method.

The steady state conversion for carbon monoxide oxidation to carbon dioxide using unwashed Pt/TiO_2 nanocomposites was measured for samples with varying W_0 (70, 150, and 200), and are shown in Figure 4a. These samples had a Pt loading of 0.5%, 1.5%, and 1.8% by weight, respectively. CO oxidation was examined over a temperature range of 70−250 °C. The conversion reached a maximum at ~150

(41) Marco, J. F.; Cuesta, A.; Gracia, M.; Gancedo, J. R.; Panjan, P.; Hanzel, D. *Thin Solid Films* **2005**, *492*, 158–165.

°C, and the extent of conversion increased with increased Pt loading as expected.

Figure 4b shows that increasing aqueous content, which increases the specific surface area of the support, does not have a very significant effect on the activity of the composites (all the composites had an overall Pt loading of 1.7%, and for these experiments, were washed). We conclude that for our highly interconnected, patterned samples, the doubling in specific surface area does not expose additional catalyst to the reactants.

The catalytic activity of our structured nanocomposites is compared to that of a commercially available TiO_2 support XT 25376 (St. Gobain-Norpro) impregnated to an equivalent Pt loading of 1.8%, using wet impregnation (refer to Supporting Information for the wet impregnation method used). Our unwashed material performed equivalently despite our nanocomposites having a fourfold *lower* specific surface area than the commercial samples (see Figure 4c).

There is a marked difference in the performance of the catalysts between washed and unwashed samples, both with Pt loading of 1.8%. This is also shown in Figure 4c. The conversion versus temperature curve shifts noticeably toward lower temperatures, reaching a maximum conversion at 100 °C for the washed sample compared to 150 °C for the unwashed one. This is a clear indication of the effectiveness of our preparation method.

These results can be understood further by examining data from the chemisorption study. The active catalyst surface area for the commercial sample is 102.20 m^2/g Pt with a 41.37% metal dispersion. When unwashed, our composite had an active catalyst surface area of 58.97 m^2/gm Pt with a 23.87% metal dispersion whereas our washed sample had an active surface of 134.76 m^2/g with a 54.56% metal dispersion. We believe that our synthesis method naturally produces well-distributed and small Pt nanoparticles. The NaCl produced as a byproduct in one of the reaction steps tends to block some of the active sites on Pt. Washing helps to remove that NaCl, thus allowing a higher active surface area and a better Pt dispersion.

We propose that the higher efficacy in our samples is also due to lower mass transfer resistance for the reactants as well as the products in the highly organized interconnected macro- and micropores and the presence of well-separated Pt nanoparticles. This explanation is supported by prior work showing increased effective mass diffusivity through a patterned highly connected porous network when compared with a random one.[42] Therefore, even the unwashed sample shows an advantage over the commercial sample. Washing improves the active catalytic surface area significantly making our nanocomposite a much better choice than its commercial counterpart.

Conclusions

We have demonstrated a new and versatile surfactant template route to synthesize highly organized nanostructured TiO_2 supports loaded with Pt nanoparticles. The TiO_2 support has a hexagonally organized porous structure with a bimodal pore diameter distribution of mesopores (∼3−14 nm) and macropores (∼20−250 nm). The organization of the solid mimics the underlying structure of the surfactant template. The Pt nanoparticles are well-dispersed on the surfaces of the TiO_2 support. Even though our nanocomposites have a low specific surface area, they exhibit a catalytic activity much better than that of a commercial catalyst for the carbon monoxide oxidation reaction. We attribute this to the lower mass transfer resistance and more available active sites on the catalyst because of the well-organized and interconnected pore structure. Apart from catalysis, such highly organized structures could be useful semiconductor material for photovoltaics and sensors.

Acknowledgment. This work is supported by a 2005 Honda Initiation Grant, the NSF (CBET 0619440, 0730392 to A.B., 0438463 to V.T.J., and DMR 0519081 to G.R.), the University of Rhode Island Transportation Research Center, and a URI Graduate Fellowship to J.S. We thank E. Wujcik, A. Javier, and K. Shukla for technical support.

Supporting Information Available: Wet impregnation technique used for loading commercial support with Pt nanoparticles and the EDS analysis for our patterned nanocomposite materials (PDF). This material is available free of charge via the Internet at http://pubs.acs.org.

CM8014034

(42) Mezedur, M. M.; Kaviany, M.; Moore, W. *AIChE J.* **2002**, *48*, 15–24.